

# A Biodegradable Piezoelectric Sensor for Real-Time Evaluation of the Motor Function Recovery After Nerve Injury

Yizhu Shan, Engui Wang, Xi Cui, Yuan Xi, Jianying Ji, Junlin Yuan, Lingling Xu,\*  
Zhuo Liu,\* and Zhou Li\*

Nerve injury can lead to defects in related motor functions. It is critical to achieve long-term and convenient real-time evaluation of motor function recovery status during nerve injury repair. In this study, an implantable PLLA/BTO piezoelectric sensor (PBPS) with good biodegradability and biocompatibility for real time evaluation of the motor function recovery after nerve injury is developed. PLLA fibers doped with BTO are employed as piezoelectric material in PBPS, which can convert the biomechanical signals generated by motion into electrical signals. PBPS can be implant simultaneously with commonly used tissue scaffolds for treatment in the rats with sciatic nerve injury. The linearity of the pressure and the output voltage of PBPS is  $\approx 0.9445$ . For the evaluation effectiveness, as the treatment process progresses, the signals generated by PBPS exhibited good consistency with EMG signals, indicating effectively evaluation of the motor function. Moreover, the integration of PBPS and wireless module can break the limitations of time and space for sensing and realize wireless evaluation of motor function in rat. The implantable sensor based on PBPS may bring new ideas for the development of implantable bioelectronics.

## 1. Introduction

Nerve injury can cause atrophy and degeneration of the muscle tissue innervated by the injured nerve, leading to defects in related motor functions.<sup>[1]</sup> Due to the complexity of the nervous system, nerve repair is difficult and time-consuming. At present, the main method used for evaluating motor function after nerve injury is to measure electromyographic (EMG) signals, which usually requires the connection of EMG electrodes and recording devices.<sup>[2]</sup> However, on account of the limitations of time and space, it is difficult to achieve long-term and convenient real-time evaluation of motor function. Therefore, it is necessary to explore and develop real-time and convenient methods for evaluating motor function to assist in the process of nerve repair.

The force electric conversion process during the movement provides a good idea for

Y. Shan, E. Wang, X. Cui, L. Xu, Z. Li  
Beijing Institute of Nanoenergy and Nanosystems  
Chinese Academy of Sciences  
Beijing 100083, China  
E-mail: [xulingling@binn.cas.cn](mailto:xulingling@binn.cas.cn); [zli@binn.cas.cn](mailto:zli@binn.cas.cn)

Y. Shan, X. Cui, Z. Li  
School of Nanoscience and Engineering  
University of Chinese Academy of Sciences  
Beijing 100049, China

Y. Xi, Z. Liu  
Key Laboratory of Biomechanics and Mechanobiology of Ministry of Education  
Advanced Innovation Center for Biomedical Engineering  
School of Engineering Medicine  
Beihang University  
Beijing 100191, China  
E-mail: [liuzhuo@buaa.edu.cn](mailto:liuzhuo@buaa.edu.cn)

J. Ji  
Center on Nanoenergy Research  
School of Physical Science and Technology  
Guangxi University  
Nanning 530004, China

J. Yuan  
Department of Health and Physical Education  
Jiangnan University  
Wuhan 430056, China

L. Xu  
New Cornerstone Science Laboratory  
CAS Key Laboratory for Biomedical Effects of Nanomaterials and Nanosafety and CAS Center for Excellence in Nanoscience  
National Center for Nanoscience and Technology  
Beijing 100190, China

 The ORCID identification number(s) for the author(s) of this article can be found under <https://doi.org/10.1002/adfm.202400295>

DOI: 10.1002/adfm.202400295

real-time motion function sensing.<sup>[3]</sup> The important way to achieve force-electric conversion is through the “smart materials” – piezoelectric materials.<sup>[4]</sup> Piezoelectric materials can generate electrical signals when subjected to deformation, and deformation when driven by electricity. Their characteristics make them widely used in various electronic products, such as generators, transducers, etc.<sup>[5]</sup> Common piezoelectric materials are mostly piezoelectric ceramic materials with high piezoelectric performance, such as lead zirconate titanate (PZT), potassium sodium niobate (KNN), lead-free barium zirconate titanate (BZT), as well as piezoelectric polymer materials commonly used in the preparation of flexible electronic devices, such as poly(vinylidene fluoride) (PVDF) and poly(vinylidene fluoride-trifluoroethylene) (PVDF-TrFE).<sup>[6]</sup> At present, sensor devices made of piezoelectric materials have been widely used in the biomedical field, including the sensing of in vivo blood pressure, intracranial pressure, and cardiac pressure.<sup>[7]</sup> To achieve good sensing effects in biomedical applications, the sensors usually need to be implanted and directly in contact with tissues or organs. This requires sensors to have moderate flexibility to avoid tissue damage caused by modulus mismatch, and excellent biocompatibility.<sup>[8]</sup> In addition, implantable sensor for short-time working should be biodegradability to avoid secondary surgical removal and reduce the risk of surgical invasiveness.<sup>[9]</sup>

Therefore, choosing a material that combines flexibility, degradability, and piezoelectric performance is the key to developing a new generation of implantable biomedical sensors. Poly-L-lactic acid (PLLA) is a Food and Drug Administration (FDA) of USA approved implantable biodegradable polymer that can exhibit certain piezoelectric properties through specific preparation methods.<sup>[10]</sup> When PLLA materials undergo a certain degree of directional stretching, the main chains of PLLA molecules would be arranged in a directional manner, and the crystal structure of the molecules would also change from  $\beta$ -crystal and  $\alpha'$ -crystal into electroactive  $\alpha$ -crystal. When deformed, the dipole of the carbonyl group extending from the main chain (COC) of PLLA will rotate slightly and vibrate in the direction perpendicular to the main chain, causing a change in molecular polarization and generating a potential in the  $d_{14}$  direction.<sup>[11]</sup> The simplest way to prepare piezoelectric PLLA films is thermal stretching, but the materials prepared by this method are usually not flexible enough or have poor reproducibility.<sup>[12]</sup> In recent years, researchers have prepared PLLA fibers with flexibility and good directionality by using electrospinning.<sup>[13]</sup> Although PLLA fiber meet the basic requirements for biomedical sensing, its piezoelectric coefficient is smaller compared to most commercial piezoelectric materials, resulting in unsatisfactory sensing output signals, which greatly limits its further clinical application as the main material for implantable sensor devices. To improve the piezoelectric response performance of PLLA, most studies control the stacking direction and thickness of PLLA fibers, but this greatly affects their flexibility and size as sensing materials. Meanwhile, the filling of inorganic nanoparticles may be a good solution. By filling with inorganic piezoelectric nanoparticles such as barium titanate (BTO), iron oxide ( $\text{Fe}_2\text{O}_3$ ), and zinc oxide (ZnO), the electromechanical coupling performance of PLLA composite materials can be enhanced while maintaining good flexibility.<sup>[14]</sup> Among them, BTO nanoparticles (BTO NPs) are widely used in the biomedical field due to their excellent piezoelectric catalytic effect, including tu-

mor treatment,<sup>[15]</sup> nerve stimulation,<sup>[16]</sup> etc., confirming their excellent biocompatibility and metabolizability. Due to the fact that the piezoelectric effect generated by BTO NPs is concentrated in the  $d_{33}$  direction, doping BTO NPs into PLLA will increase the possibility of the electrical potential generated by the whole materials in more directions and improve the piezoelectric output.

In this study, we constructed a biodegradable PLLA/BTO piezoelectric sensor (PBPS) for wireless evaluation of the motor function recovery after nerve injury. After uniformly dispersing BTO NPs in the PLLA solution, we prepared oriented PLLA/BTO fiber films through electrospinning. By characterizing fiber films with different doping ratios and considering factors such as biocompatibility, the optimal doping ratio was determined. And the materials prepared at this ratio were characterized, verifying their excellent piezoelectric performance. We chose the flexible material polycaprolactone (PCL), which is also biodegradable and has good biocompatibility, as the packaging layer, and the degradable molybdenum (Mo) as the electrode layer to form a sandwich structure with PLLA/BTO fiber films for PBPS. Through in vitro testing, the  $V_{\text{max}}$  of 1.8 V and  $I_{\text{max}}$  of 30 nA by PBPS can be achieved, and it has a good electromechanical response relationship. We evaluated the motion sensing effect in a rat sciatic nerve injury model. As the repair process progresses, the output signal of the sensor gradually increased and had similar responsiveness to traditional electromyographic (EMG) testing signals, which proved that PBPS has the ability to evaluate the recovery of motor ability after nerve injury. We hope that this wireless sensing system based on PBPS can bring new ideas for the development of implantable biomedical electronic devices in the future.

## 2. Results

### 2.1. Overview of the PBPS Based Wireless Evaluation of Motor Function Recovery

The basic structure and working mode of PBPS in vivo were shown in **Figure 1a,b**. The PBPS composed of PLLA/BTO fibers, Mo electrodes, and PCL films was implanted subcutaneously in the leg of a rat sciatic nerve injury site during therapeutic tissue engineering scaffold implantation surgery, and connected to a wireless module worn on the back. When rats moved their legs, the deformation of PBPS happened, which in turn generated the electrical signal output driven by the movement. The voltage signal was then transmitted to the real-time display module through a wearable Bluetooth module, achieving wireless evaluation of motor function recovery. The main structure of PBPS was PLLA/BTO fibers, which were mainly prepared by electrospinning (**Figure 1c**), and the oriented fibers obtained were loaded with BTO NPs. It can be seen from the photos that PBPS took on a flower shape and had a certain degree of flexibility.

### 2.2. Characterization of PLLA/BTO Fibers

Due to the small size and accumulation of a large amount of charge on the surface of the particles, BTO NPs are prone to agglomeration.<sup>[17]</sup> Therefore, during the preparation process, we fully carried out dispersion by ultrasonic to minimize the agglomeration of BTO NPs and evenly distributed them on PLLA

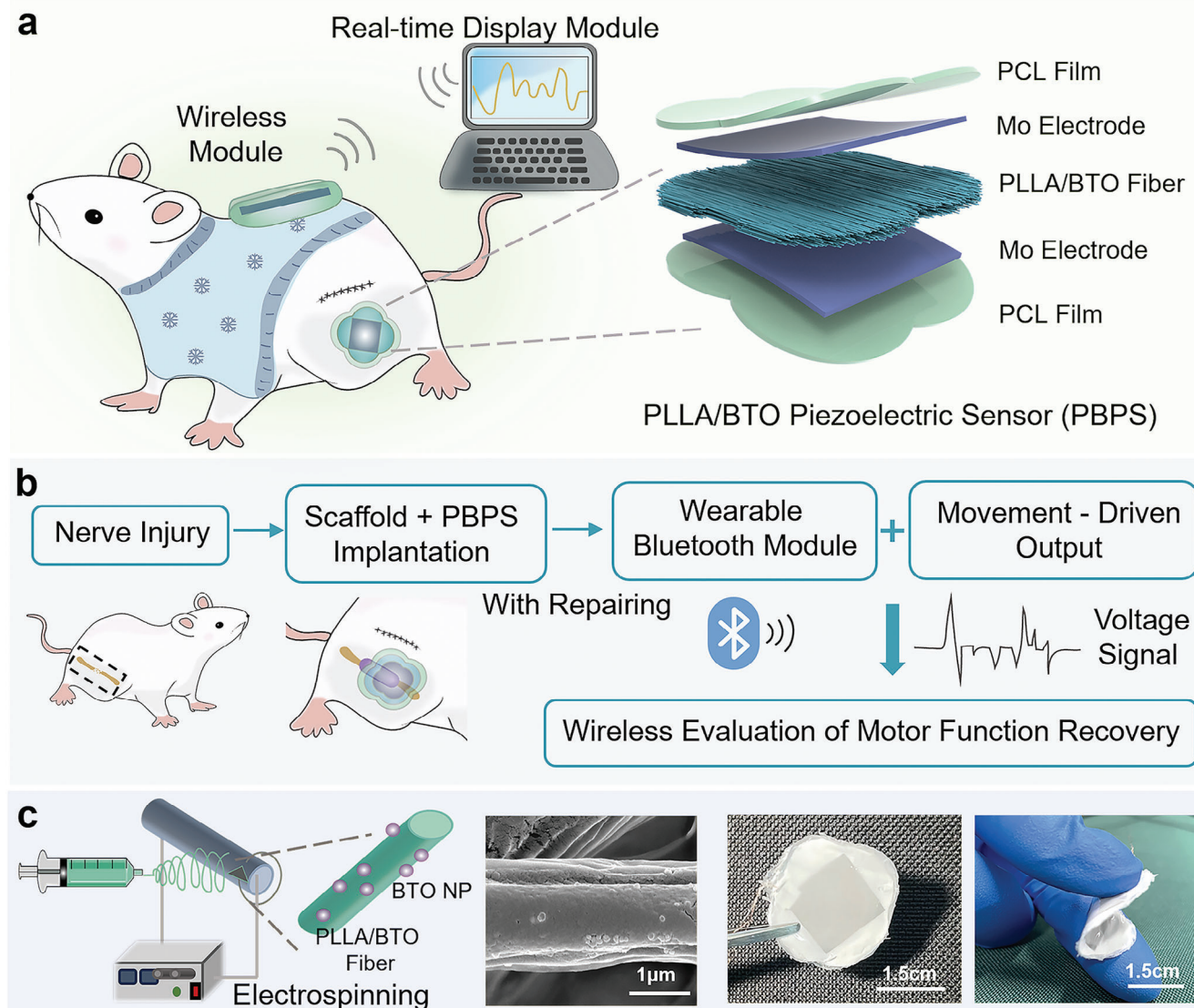


**Figure 1.** Schematic illustration of PBPS structure and working diagram. a) Schematic diagram of PBPS in rats and the composition and structure of PBPS. b) A work flowchart of PBPS. c) Preparation method, microstructure, and real product photo of PBPS.

fibers. In order to investigate the optimal proportion of BTO doped in PLLA, we prepared PLLA/BTO fiber films with gradient doping ratios of 0%, 5%, 10%, and 20%, respectively. By observing the surface morphology of these fiber films by scanning electron microscope (SEM) (Figure 2a), we found that each doped proportion of fibers had a relatively good directional arrangement, and scattered BTO NPs adhered to the fibers could be observed. By zooming in on the local area of the fiber, it can be seen that as the doping ratio increases, the number of scattered BTO particles on the fiber also gradually increased. However, as the proportion of BTO doping increases, adhesion gradually occurs between the fibers. Although all materials have undergone sufficient drying and volatilization, the adhesion of the fiber films with a 20% doping ratio of BTO NPs was still severe. In the process of experiment, we found that with the increase of doping ratio of BTO NPs, the volatility of the spinning solution using hex-

fluoroisopropanol as the solvent was greatly reduced. We speculate that the dispersion of BTO NPs in the solvent may slow down the diffusion movement of solvent molecules, thereby increase the stability of the entire working solution, and lead to the adhesion between the fibers due to incomplete solvent evaporation. In order to fully demonstrate the doping condition of BTO NPs in PLLA fibers, we used energy dispersive spectroscopy (EDS) spectroscopy to characterize the local element distribution of PLLA fibers with a 10% doping ratio of BTO NPs. From Figure 2b, it can be seen that the main elements C and O that makeup PLLA coincided with the main morphology of the fibers, and the main elements Ba and Ti of BTO NPs were scattered on the fibers.

Next, we measured the piezoelectric coefficient  $d_{33}$  and  $d_{14}$  of fiber films with different doping ratios. After directional stretching through electrospinning, the piezoelectricity of PLLA fibers mainly come from the stretching vibration of carbonyl

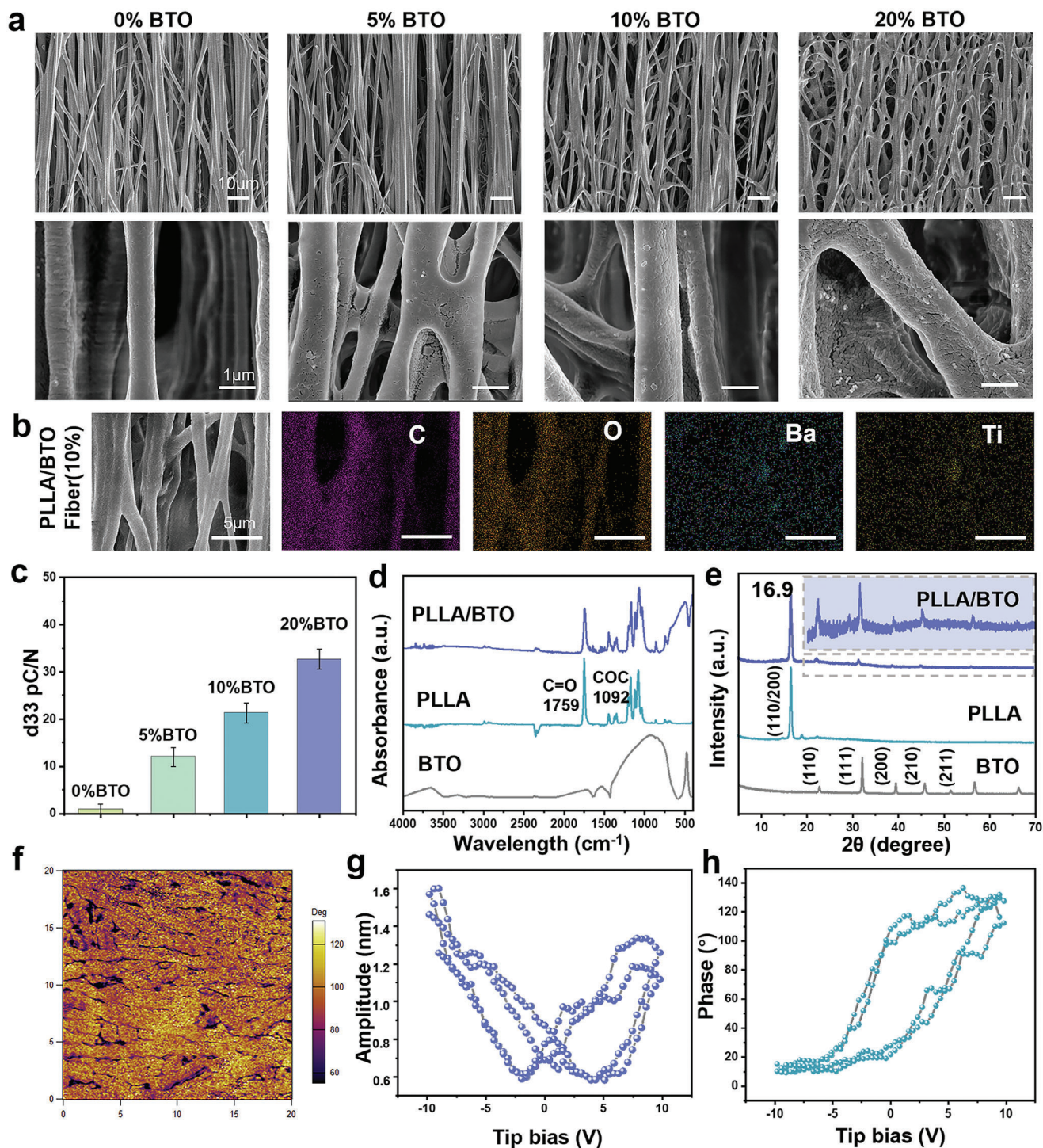


**Figure 2.** Characterization of PLLA/BTO fiber. a) Photograph of the morphology of the PLLA/BTO fiber of different ratio by SEM. b) EDS results of the PLLA/BTO fiber with the doping ratio of 10%. c) The piezoelectric coefficient of  $d_{33}$  of different doping ratio of PLLA/BTO fiber. ( $n = 3$ ) d) The result of FTIR test of BTO NPs, PLLA fiber, and PLLA/BTO fiber. e) The result of XRD test of BTO, PLLA fiber, and PLLA/BTO fiber. f) PFM phase map of the PLLA/BTO fibers. g) Amplitude curve and h) phase curve of PLLA/BTO fiber obtained by PFM.

groups extending from the main chain, and this change in molecular polarization is mainly reflected in the  $d_{14}$  direction.<sup>[18]</sup> The result in Figure S1 (Supporting Information) showed that the doping of BTO did not have a significant impact on the value of  $d_{14}$ . Without doping BTO NPs, the  $d_{33}$  coefficient exhibited by the fiber material was very small. Due to the polarization of BTO NPs, their piezoelectricity is mainly reflected in the  $d_{33}$  direction. Therefore, as the doping ratio increases, the  $d_{33}$  piezoelectric coefficient of the fiber films increased ( $12 \pm 2$  pC N<sup>-1</sup> at 5% BTO,  $21.33 \pm 2.08$  pC N<sup>-1</sup> at 10% BTO, and  $32.67 \pm 2.52$  pC N<sup>-1</sup> at 20% BTO, Figure 2c). Although fiber films with a 20% doping ratio exhibit high piezoelectricity, the adhesion between their fibers may represent the presence of residual organic solvents. On the other hand, high levels of BTO NPs implanted in the body may lead to metabolic difficulties. Taking into account the above factors, we have chosen a 10% doping ratio of BTO NPs as the condition for subsequent experiments.

The internal composition of the PLLA/BTO film were further tested by Fourier transform infrared (FT-IR) (Figure 2d). The characteristic peaks appearing at 1092 and 1759 cm<sup>-1</sup> in the infrared spectrum of PLLA film represented the C=O and COC functional groups. The infrared spectrum of BTO NPs exhibited a characteristic absorption peak at 500 cm<sup>-1</sup>. In PLLA/BTO materials, both characteristic absorption peaks of PLLA and BTO can be observed, indicating the successful doping of BTO in PLLA. X-Ray Diffraction (XRD) can effectively analyze the crystallization of materials. As shown in Figure 2e, we used XRD to characterize BTO NPs, PLLA fibers, and PLLA/BTO fiber films. The XRD peaks of BTO NPs were very well overlapped with the standard ones. The PLLA films exhibited an extremely strong diffraction peak at  $\approx 16.9^\circ$ , corresponding to the 110/200 crystal plane of PLLA, and representing the main formation of  $\alpha$ -crystal of PLLA after electrospinning.  $\alpha$ -crystal of PLLA has electrical activity, indicating that the PLLA fiber we prepared has a certain degree of piezoelectricity. In the XRD data of PLLA/BTO fiber film materials, we can simultaneously observe the characteristic peaks of BTO and characteristic peaks of  $\alpha$ -crystal PLLA that indicated that the crystallization of PLLA and BTO in PLLA/BTO materials did not affect each other, and each exhibit certain piezoelectric properties. Due to the research exploring the effect of 10% to 20% BTO doping ratio on the crystallization performance of the piezoelectric materials,<sup>[19]</sup> we also investigated the crystallization performance of PLLA between this doping ratio. We selected materials with a 15% doping ratio for XRD testing, and the results showed that the half width of the diffraction peak at  $16.9^\circ$  was  $0.9845 \pm 0.004$  for 10% BTO, while the half width was  $0.9799 \pm 0.002$  for 15% BTO (Figure S2, Supporting Information). There showed no significance between different doping ratio and represented that the doping of BTO did not significantly affect the crystallization performance of PLLA.

We then evaluated the piezoelectric responsiveness of the prepared PLLA/BTO fiber films by PFM. The morphology of the material were characterized, the amplitude and phase changes of the probe through the contact between the PFM probe and the sample surface were tested. Under a bias voltage of 10 V, oriented fibers were observed (Figure S3, Supporting Information), and the color inside the fibers is almost uniform, suggesting their existence in a single domain state (Figure 2f). The data in Figure 2g indicates that under applied bias, the dipole of the material ro-

tated, with maximum amplitudes reaching 1.62 and 1.35 nm, respectively. In addition, the hysteresis loop tested under PFM also indicates that PLLA/BTO materials have good piezoelectricity (Figure 2h).

### 2.3. Characteristic and Performance of PBPS

In this study, we chose the flower shape as the shape of the PBPS. We speculate that compared to traditional shape of the sensor, the round corners of flower shape sensor cause less damage to the tissue during contact. On the other hand, the flower shape may show better adaptability and more sensitive sensing of the movement, resulting in a larger output. The Comsol Multiphysics were applied to simulate the potential changes generated by force on square, round, and flower shaped sensors of the same area (Figure 3a), and the result is consistent with the conjecture. During the operation of PBPS, it is mainly subjected to two modes of force, namely pressing and bending. The working principle of PBPS under these two states is explained in Figure 3b, the internal dipoles are in equilibrium when PBPS is not subjected to external forces. When PBPS is compressed by external mechanical motion, the dipoles rotate, and the generated electrons flow through the external circuit, generating a current. When PBPS is bent by external forces, dipole rotation also occurs, generating a certain amount of current. By connecting PBPS to external circuits, alternating electrical signals can be displayed. The simulation of the output of PBPS under two force modes was shown in Figure S4 (Supporting Information).

For the evaluation of the performance of PBPS in vitro, we first tested the maximum output of PBPS. The resulting of the maximum output of open-circuit voltage ( $V_{oc}$ ), short-circuit current ( $I_{sc}$ ), and short-circuit transferred charge ( $Q_{sc}$ ) under the motivation of a liner motor were  $\approx 1.8$  V, 30 nA, and 18 nC, respectively. It is worth mentioning that we compared the output of polarized PBPS and unpolarized PBPS under the same force. The results in Figure S5 (Supporting Information) showed that the polarization operation greatly improved the performance of PBPS. Then we applied a reciprocating and quantitative force to PBPS by Mark10, and measured the output voltage of PBPS under gradient force. Under the forces of 3, 20, 42, and 87 N, the  $V_{oc}$  of PBPS were  $0.51 \pm 0.02$ ,  $0.91 \pm 0.04$ ,  $1.42 \pm 0.03$ , and  $2.16 \pm 0.02$  V, respectively. In addition, we also performed linear fitting on this test result, and the results showed that the electromechanical coupling of PBPS has a certain degree of linearity ( $R^2 = 0.9445$ , Figure 3g). In addition to the output under pressure, we also tested the performance of PBPS under bending. The experimental photos and output results were shown in Figure S6 (Supporting Information). Due to the long process of nerve repair, PBPS requires a longer service life, and maintaining its stability is crucial. We then evaluated the cyclic stability of PBPS under a force of 1 Hz. After >1500 times compression and recovery experiments, the  $V_{oc}$  of PBPS showed almost no attenuation and remained stable at  $\approx 0.7$  V (Figure S7, Supporting Information).

### 2.4. The Biocompatibility and Biodegradability of PBPS

For implantable electronic devices, biocompatibility is crucial. Before conducting animal experiments, we tested a

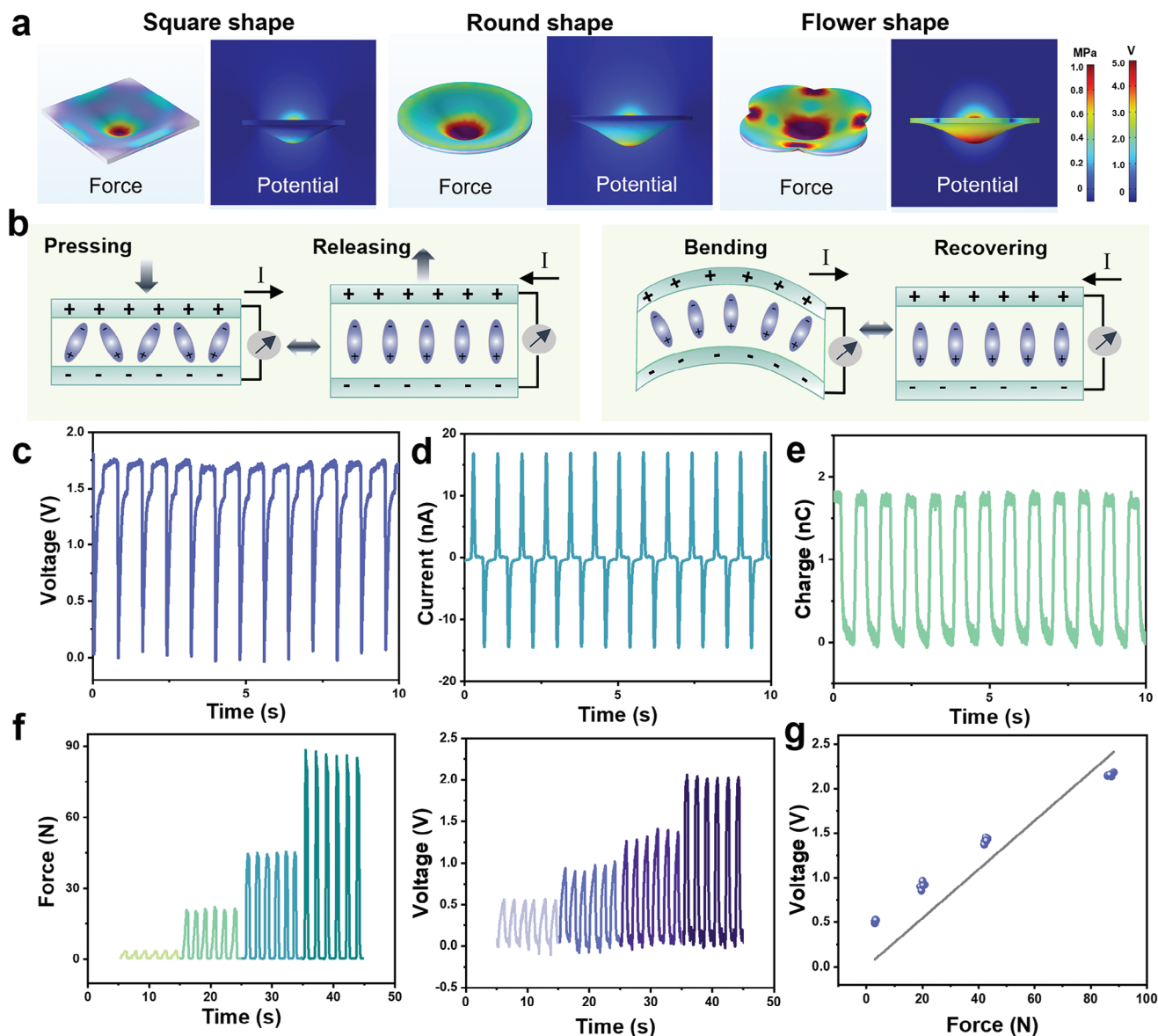


**Figure 3.** Performance of PBPS output. a) Simulation of different shape of PBPS with COMSOL Multiphysics. b) Schematic of the working principles of PBPS under pressing and bending. c) Maximum output of the voltage, d) current, e) charge of PBPS. f) The gradient forces applied on PBPS by Mark-10 and the responsive voltage output. g) The result of the linear fitting of the force and voltage output of PBPS.

comprehensive evaluation of the biocompatibility of the two main materials in PBPS (PCL and PLLA/BTO/Mo coated with Mo electrodes (PLLA/BTO/Mo)). In terms of cell compatibility, both PCL and PLLA/BTO/Mo showed no difference in cell viability compared to the control group (cell culture plate) in the live death staining experiment (Figure 4a,b). In addition, the CCK8 test results further confirmed the good cell compatibility of the two materials (Figure 4c). PBPS needs to be implanted subcutaneously for a long-time during application, so evaluating its blood and tissue compatibility is an important prerequisite for safe in vivo application. We evaluated the blood compatibility of positive control (water), negative control (PBS), and two materials using hemolysis experiments. The results showed that the positive control group showed significant hemolysis, while the

hemolysis in the PCL and PLLA/BTO/Mo groups was consistent with the negative control group, and no hemolysis was observed (Figure 4d). After implanting PCL and PLLA/BTO/Mo materials subcutaneously in SD rats for one month, samples were taken from the skin and subcutaneous tissue near the implantation site and the sections were conducted with HE staining. The results in Figure 4e indicated that the two materials did not form large fibrous cysts subcutaneously and did not cause significant inflammatory reactions, which confirmed the tissue compatibility of PBPS. Furthermore, implantable sensor components should have biodegradability to avoid secondary surgical removal and reduce the risk of surgical invasiveness. Due to the fact that the main materials of PBPS – PLLA and PCL, are both FDA approved excellent biodegradable implantable biomedical

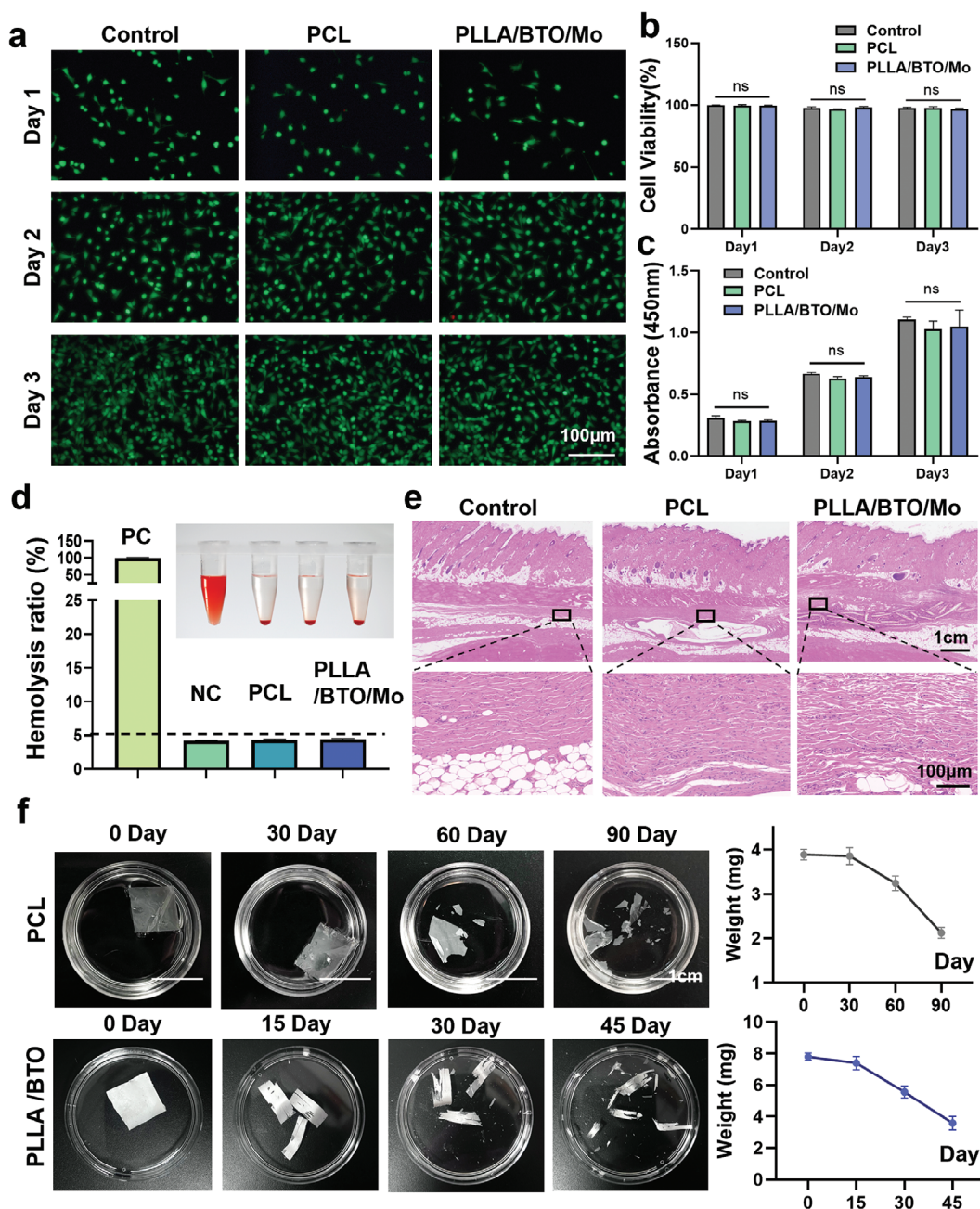


**Figure 4.** Biocompatibility and biodegradability evaluation of PBPS. a) The result of the Live/Dead staining of the L929 cells of the control group, PCL group, and PLLA/BTO/Mo group at day 1, day 2, and day 3. b) Statistical result of the cell viability of Live/Dead staining. ( $n = 3$ ) c) The absorbance of CCK8 result of the cells of the control group, PCL group, and PLLA/BTO/Mo group at day 1, day 2, and day 3. ( $n = 3$ ) d) The result of the hemolysis ratio of the positive control, negative control, PCL group, and PLLA/BTO/Mo group. ( $n = 4$ ) e) The photographs of HE staining results of the control group, PCL group, and PLLA/BTO/Mo group. f) The photographs of the degradable condition of PCL films and PLLA/BTO films at different stages and the weight at different time ( $n = 3$ ).

materials, their biodegradability has been confirmed. In this study, we tested the biodegradability of PCL that is the encapsulation layer of PBPS and PLLA as the main piezoelectric materials. Since both materials have long degradation cycles, we used accelerated degradation experiments to characterize the degradability of the materials. For the PCL material, we used heating to accelerate the degradation. For PLLA/BTO material, we referred

to the way in the literature<sup>[9c,20]</sup> and utilized the dual intervention of ultrasound and heating for the degradation experiments of PLLA/BTO films. The results showed that PCL and PLLA/BTO gradually exhibited degradation after stable operation for at least 1 month (Figure 4f). We also characterized the hardness of the PCL film and PLLA/BTO film that make up PBPS. The data in Figure S8 (Supporting Information) showed that the Young's

modulus of the membrane composed of PBPS is relatively low (PLLA/BTO/Mo film was  $\approx 2.13 \pm 0.16$  MPa and the PCL film was  $\approx 0.93 \pm 0.06$  MPa), close to that of biological tissues. We also evaluated the flexibility of PBPS. The data in Figure S9 (Supporting Information) showed the definition of the bending degree. The results demonstrate that the bending degree of PBPS can reach 55% and verified the flexibility of PBPS.

## 2.5. In Vivo Sensing Performance of PBPS

At present, the main method used for evaluating motor function after nerve injury is to measure EMG signals, which usually requires the connection of electromyographic electrodes and EMG recording devices for recording.<sup>[21]</sup> Therefore, limited by the location and time of use, it is impossible to achieve long-term and convenient real-time evaluation of motor function, and thus unable to provide reference data for the next stage of treatment in nerve repair in a timely manner. In this study, we proposed to implant PBPS subcutaneously on the affected side during therapeutic nerve scaffold implantation surgery, achieving integrated diagnosis and treatment of nerve injury repair and wireless motion evaluation (Figure 5a).

To evaluate the ability of PBPS based motion sensing to evaluate motor function at different stages of neural repair, we first tested wired sensing signals in the early (2 weeks), middle (6 weeks), and terminal (12 weeks) injury stages of neural repair (Video S1, Supporting Information). From the data in Figure S10 (Supporting Information), it can be seen that as the treatment process progressed, the peak sensing signal of PBPS also gradually increased. To further demonstrate the potential of the PBPS we prepared in evaluating motor function rehabilitation after nerve injury, we synchronously tested the EMG signals and PBPS output signals of rats with sciatic nerve injury at these three repair stages. The experimental process was shown in Video S2 (Supporting Information). We presented representative EMG signals and PBPS sensing signals from the same time period in Figure 5b. We can see from the data that with the passage of treatment time, the peak value of EMG signals gradually increased, indicating a gradual recovery of motor function, which further reflected the repair of damaged nerves. The peak values of the PBPS signal tested synchronously during testing also showed a consistent pattern with the EMG signal, indicating that PBPS can achieve good effect of motor function evaluation. It is worth noting that from the perspective of signal correspondence at the same time, the PBPS signal and EMG signal we tested synchronously showed a high degree of response consistency. Furthermore, we utilized short-time Fourier transform to perform time-frequency analysis on a portion of the test signal to explore the variation of signal frequency over time and the instantaneous frequency and amplitude at each moment. The results were listed on the right side of Figure 5b. In the time-frequency analysis results, EMG signals and PBPS signals exhibited good consistency in time-frequency response, which further proves that PBPS based sensing systems can play a role similar to EMG evaluation in motor function recovery evaluation after nerve injury.

The Video S3 (Supporting Information) showed the process of monitoring the movement process of rats using a wireless

sensing system constructed by Bluetooth module and PBPS. The wireless sensing system we have constructed mainly consists of three parts: an implantable sensing unit with PBPS as the main body, a wearable wireless module with wireless transmission module as the main body, and a mobile device display end for receiving wireless transmission signals outside the body. The PBPS inside the body was connected to the wireless module worn outside the body through wires led out from PBPS, and the wires were led subcutaneously to the back of rats. When the movement of the rat's leg occurred, PBPS would then convert the mechanical force of deformation into electrical signals and transmit them to the wireless Bluetooth module worn on the rat's back. Then the wireless module wirelessly transmitted electrical signals to mobile display devices through circuits, thereby achieving wireless real-time monitoring of motion signals. Figure 5c and d respectively demonstrated the captured photos of the real-time signals recorded by the real-time display module for rats in both rest and moving states, as well as the output signals recorded for rats in continuous motion over a period of time.

## 3. Conclusion

In this study, we constructed a biodegradable piezoelectric sensor for real-time evaluation of the motor function recovery after nerve injury and demonstrated its potential application in rats. First, by comprehensively considering the application requirements, we selected PLLA fiber with biocompatibility, biodegradability, and certain piezoelectric properties as the main materials for the sensors. This material is also approved by the FDA for use in the development of biomedical devices. In order to improve the piezoelectric performance of the sensor, we have modified the PLLA fiber. By optimizing the experimental conditions, we achieved excellent piezoelectric properties of the composite material by doping BTO, an inorganic nanoparticle, during the preparation process of PLLA fibers. For the assembling of PBPS, we have chosen FDA-approved PCL as the packaging layer material, achieving overall safety and biodegradability. Moreover, we prepared PBPS in the shape of flowers for avoidance of physical stimuli and significant deformation under the same force. The maximum output voltage of the final prepared PBPS can reach 1.8 V and the PBPS exhibited good linearity. In addition, we demonstrated the application effect of PBPS in a rat model of sciatic nerve injury. Compared with traditional EMG testing methods, signals generated by PBPS were in conformity with EMG signals. Finally, PBPS based biodegradable piezoelectric sensors can achieve wireless evaluation of motor function recovery after nerve injury. We will evaluate the long-term efficacy and stability of PBPS in vivo and conduct experiments in a larger number of samples in future research. In summary, the motion sensing system we have developed provides references for the development of next-generation wireless, biodegradable implantable bioelectronic devices.

## 4. Experimental Section

**Materials:** PLLA (Mw 260 000) was purchased from Daigang Biomaterial (China). PCL powder (Mw 6500) was purchased from Aladdin (China). BTO nanopowder was obtained from Sigma-Aldrich (Germany).

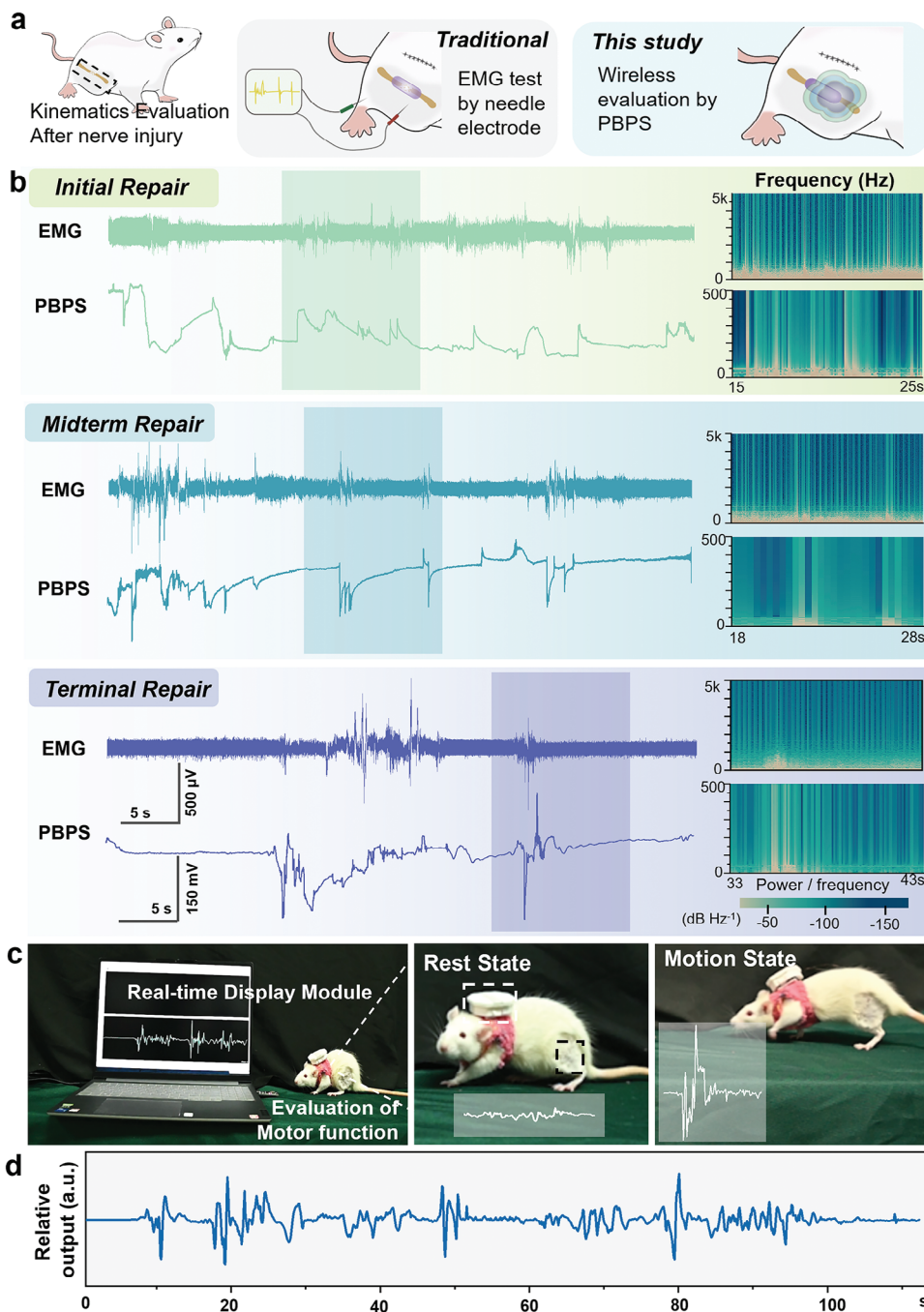


**Figure 5.** Evaluation of the motion function in vivo. a) Schematic of kinematics evaluation after nerve injury with traditional EMG test and wireless evaluation by PBPS in this study. b) EMG signals and signals tested by PBPS at three different stages of repair, the right of the results showed the time-frequency analysis of the signals of the shaded portion. c) Photographs of the wireless evaluation of motor function of the rats. The pictures showed the rest state and motion state of the rats and the responding signals. d) Relative output signals recorded by the real-time display module.

Hexafluoroisopropanol (HFIP) solution and dichloromethane solution were purchased from Aladdin (China). Dulbecco's Modified Eagle Medium (DMEM), PBS, trypsin, Calcein-AM/PI double-labeled kit, and CCK-8 solution were purchased from Solarbio (China). The SD rats were purchased from Beijing Vital River Laboratory Animal Technology Co. Ltd (China).

**Preparation of PLLA/BTO Nanofiber Films:** The main part of PBPS – piezoelectric PLLA/BTO nanofibers by electrospinning was prepared. In order to improve the dispersibility of BTO NPs, BTO NPs were first dispersed in the hexafluoroisopropanol solution under ultrasound. Then add PLLA powder (10%) to the solution and stir overnight until completely dissolved. Before spinning, the solution was dispersed under ultrasound

for another 10 min. A 5 mL of syringe containing a mixed solution of PLLA/BTO was placed on the electrospinning machine. A positive high voltage of 13 kV was added to the needle of syringe 21, and a negative high voltage of 3 kV was added to the receiving roller. The rotational speed of the rotary cylinder was set to 1000 r min<sup>-1</sup>, the pushing speed of the syringe to 1 mL h<sup>-1</sup>, the receiving distance to 10 cm, and the receiving time to 1.5 h. After spinning, place the spinning film overnight in a fume hood to allow the solvent to fully evaporate. Next, the spinning films were clamped with glass sheets and placed in a 130 °C oven for annealing for 4 h, then let it cool naturally and carefully remove the material from the glass sheet to obtain the PLLA/BTO nanofiber films. Before characterizing the material, the PLLA film was polarized by high-voltage corona polarization (Trek 610E, USA). The high voltage was set as 15, 5 kV and the duration was set as 10 min. SEM (Nova NanoSEM 450, FEI, Crech) was used to observe the surface morphology of the films with different doping ratios. Then, infrared spectroscopy (VERTEX80v, Bruker, Germany) was applied to characterize the composition of the films, and XRD (Xpert3, PANalytical, Poland) was used to test the crystallization of the fiber membrane. For the characterization of the piezoelectric properties of fiber membranes, it was first used a d<sub>33</sub> piezoelectric coefficient measuring instrument to characterize the piezoelectric coefficients of the films with different doping ratios. Then, nanoscale polarization imaging and local switching spectra were conducted by a resonant enhanced piezoelectric force microscopy (MFP-3D-SA, Asylum Research, USA).

**Preparation of PBPS:** After bonding the prepared nanofiber film with the mask, a layer of Mo electrodes was sputtered on both sides of the film by a plasma enhanced chemical vapor deposition (Si 500D, SENTECH, Germany) for 30 min. Then, two copper wires were led out from the Mo electrodes on both sides of the film. For the preparation of the packaging layer of the sensor, dissolve PCL powder in dichloromethane solution to prepare a 20% solution. After sufficient stirring and dissolution, the PCL films were prepared by using a homogenizer in the fume hood. Finally, the PCL film of the packaging layer was sandwiched between the nanofiber films by hot pressing to form a PBPS.

**In vitro Electrical Test of PBPS:** The  $V_{oc}$ ,  $I_{sc}$ , and  $Q_{sc}$  were measured by an electrometer (Keithley 3517, USA) and recorded by an oscilloscope (LeCroy, HDO6104, USA). And the  $V_{max}$  and  $I_{max}$  were detected under the driving of a linear motor (LinMot E1100, Switzerland). For the testing of the force-electrical output relationship, the push-pull dynamometer (Mark-10, USA) to quantitatively apply forces of different sizes to PBPS was used and synchronously test the electrical output of the device. More than 1500-times of fatigue tests were conducted under a force of  $\approx 5$  N at a frequency of 1 Hz. The size of PBPS used in in vitro testing was the same as in vivo experiments.

**Biocompatibility Test of PBPS:** The leached medium of PCL films and PLLA/BTO films with Mo electrode for cell biocompatibility evaluation was prepared by incubating 100 mg sterilized materials in 50 mL standard DMEM medium at 37 °C for 48 h. The L929 cells were used for cell biocompatibility test. The cells were seeded in a 24-well cell culture plate for the two kinds of leached culture medium as the experimental group and for pristine DMEM as the control group. The cells were cultured for 1, 2, and 3 d at 37 °C under 95% air and 5% CO<sub>2</sub>. Live-dead staining of the cells was used to evaluate the morphology and vitality of the cells. After fluorescence staining of the cells at 1, 2, and 3 d, the fluorescence images of cells were observed by a fluorescence microscope (DM6000, Leica, USA) under 490  $\pm$  10 nm (live) and 545 nm (dead). To quantify the cell viability, 10% CCK-8 solution and 90% culture medium were used to incubate L929 cells for 2 h after washing the cells with 1 $\times$ PBS for three times. Then, 200  $\mu$ L of supernatant of each well was transferred into a 96-well plate. The absorbance of the solution was measured under 450 nm with a microplate absorbance assay instrument (Varioskan Lux, Thermofisher, USA).

Hemolysis experiment was conducted for the blood compatibility evaluation. 1 mL of fresh rat blood was taken into an anticoagulant tube, then added with 2 mL of PBS solution, and centrifuged at 1000 r for 5 min. The centrifugation was repeated for 4 times until the supernatant become clear and transparent and the supernatant was discarded. Then the red blood cells were resuspended in 10 mL of PBS solution as blood working solution. 200  $\mu$ L of blood working fluid and 800  $\mu$ L of material leached

solution were mixed as the experimental group, with an equal amount of blood working solution and water as the positive control (PC), and an equal amount of blood working solution and PBS as the negative control (NC) ( $n = 4$ ). After incubating at 37 °C for 4 h, the samples of each group were centrifuged at 1000 r for 5 min, and 100  $\mu$ L of the supernatant samples from each group were used to test the absorbance at 577 nm.

PCL films and PLLA/BTO films with Mo electrode were implanted subcutaneously in SD rats to observe the tissue compatibility of the materials. After one month of implantation, the skin and subcutaneous tissue were taken from the rats at the implantation site for HE section staining observation.

The degradability following the following steps was characterized. For the PCL membrane, first cut it into a size of 1  $\times$  1 cm, then place them in a culture dish and immerse it in PBS buffer solution. Place the culture dish on a heating table at 65 °C for accelerated degradation experiments, and replace with fresh PBS solution every two days. For the degradation testing of PLLA/BTO membranes, due to their long degradation cycle, an accelerated degradation method combining ultrasound and heating was adopted. The PLLA/BTO films were cut into the size of 2  $\times$  2 cm and also immersed in PBS in culture dishes and placed on a heating table. When changing the PBS solution every two days, the material was subjected to focused ultrasound stimulation with an intensity of 1 W cm<sup>-2</sup> for 10 min. At regular intervals, the materials were dried and weighed, and were taken photos for recording.

**In Vivo Study:** Animal experiments were conducted under the requirements of the Beijing Institute of Nanoenergy and Systems (2023016LZ). After anesthesia, SD rats were first subjected to a modeling experiment of sciatic nerve injury. Then, PBPSs were implanted subcutaneously on the injured leg and the wound was sutured. For the measurement of electromyographic (EMG) signals, the positive electrode was inserted into the muscle of the rat, the negative electrode was inserted subcutaneously under the ankle, and the ground electrode was placed subcutaneously away from the measurement site. The EMG signals were recorded by MP150 (Biopac, USA). For the evaluation of PBPS output in vivo, in wired testing, PBPS was connected to an electrometer for measurement; in wireless testing, PBPS was connected with Bluetooth module, and the output would be displayed on a mobile computer.

## Supporting Information

Supporting Information is available from the Wiley Online Library or from the author.

## Acknowledgements

This work was financially supported by grants from the National Key Research and Development Program of China (2022YFE0111700, 2021YFB3200600), the National Natural Science Foundation of China (T2125003, 82102231, and 82372141), Beijing Natural Science Foundation (L212010), the Fundamental Research Funds for the General Universities.

## Conflict of Interest

The authors declare no conflict of interest.

## Data Availability Statement

The data that support the findings of this study are available from the corresponding author upon reasonable request.

## Keywords

biodegradability, motion evaluation, nerve injury, piezoelectric sensor

Received: January 7, 2024  
Revised: March 1, 2024  
Published online:

- [1] S. Vijayavenkataraman, *Acta Biomater.* **2020**, *106*, 54.  
[2] L. R. Robinson, *Muscle Nerve* **2022**, *66*, 661.  
[3] M. T. Chorsi, E. J. Curry, H. T. Chorsi, R. Das, J. Baroody, P. K. Purohit, H. Ilies, T. D. Nguyen, *Adv. Mater.* **2019**, *31*, 1802084.  
[4] L. Liu, Y. Li, M. Xu, R. Tao, Q. Zhong, X. Yang, S. Lan, J. Xie, G. Chen, Y. Mao, W. Hu, *Chem. Eng. J.* **2023**, *474*, 145866.  
[5] S. Panda, S. Hajra, K. Mistewicz, P. In-na, M. Sahu, P. M. Rajaittha, H. J. Kim, *Nano Energy* **2022**, *100*, 107514.  
[6] a) S. D. Mahapatra, P. C. Mohapatra, A. I. Aria, G. Christie, Y. K. Mishra, S. Hofmann, V. K. Thakur, *Adv. Sci.* **2021**, *8*, 2100864; b) C. Chen, X. Wang, Y. Wang, D. Yang, F. Yao, W. Zhang, B. Wang, G. A. Sewvandi, D. Yang, D. Hu, *Adv. Funct. Mater.* **2020**, *30*, 2005141.  
[7] a) J. Ji, C. Yang, Y. Shan, M. Sun, X. Cui, L. Xu, S. Liang, T. Li, Y. Fan, D. Luo, Z. Li, *Adv. Nanobiomed Res* **2023**, *3*, 2200088; b) R. A. Surmenev, T. Orlova, R. V. Chernozem, A. A. Ivanova, A. Bartasyte, S. Mathur, M. A. Surmeneva, *Nano Energy* **2019**, *62*, 475; c) J. Wang, T. He, C. Lee, *Nano Energy* **2019**, *65*, 104039; d) C. Wang, Y. Hu, Y. Liu, Y. Shan, X. Qu, J. Xue, T. He, S. Cheng, H. Zhou, W. Liu, Z. H. Guo, W. Hua, Z. Liu, Z. Li, C. Lee, *Adv. Funct. Mater.* **2023**, *33*, 2303696.  
[8] a) H. Zhou, Y. Zhang, Y. Qiu, H. Wu, W. Qin, Y. Liao, Q. Yu, H. Cheng, *Biosens. Bioelectron.* **2020**, *168*, 112569; b) J. Li, C. Carlos, H. Zhou, J. Sui, Y. Wang, Z. Silva-Pedraza, F. Yang, Y. Dong, Z. Zhang, T. A. Hacker, B. Liu, Y. Mao, X. Wang, *Nat. Commun.* **2023**, *14*, 6562.  
[9] a) E. J. Curry, T. T. Le, R. Das, K. Ke, E. M. Santorella, D. Paul, M. T. Chorsi, K. T. M. Tran, J. Baroody, E. R. Borges, B. Ko, A. Golabchi, X. Xin, D. Rowe, L. Yue, J. Feng, M. D. Morales-Acosta, Q. Wu, I. P. Chen, X. T. Cui, J. Pachter, T. D. Nguyen, *Proc. Natl. Acad. Sci. USA* **2020**, *117*, 214; b) G. Yao, L. Kang, C. Li, S. Chen, Q. Wang, J. Yang, Y. Long, J. Li, K. Zhao, W. Xu, W. Cai, Y. Lin, X. Wang, *Proc. Natl. Acad. Sci. USA* **2021**, *118*, e2100772118; c) D. M. Lee, M. Kang, I. Hyun, B. J. Park, H. J. Kim, S. H. Nam, H. J. Yoon, H. Ryu, H.-m. Park, B. O. Choi, S. W. Kim, *Nat. Commun.* **2023**, *14*, 7315; d) X. Xiao, X. Meng, D. Kim, S. Jeon, B. J. Park, D. S. Cho, D. M. Lee, S. W. Kim, *Small Methods* **2023**, *7*, 2201350.  
[10] a) E. Capuana, F. Lopresti, M. Ceraulo, V. L. Carrubba, *Polymers* **2022**, *14*, 1153; b) F. Ebrahimi, H. Ramezani Dana, *Int. J. Polym. Mater. Polym. Biomater.* **2022**, *71*, 1117.  
[11] Y. M. Yousry, V. K. Wong, R. Ji, Y. Chen, S. Chen, X. Zhang, D. B. K. Lim, L. Shen, K. Yao, *Adv. Funct. Mater.* **2023**, *33*, 2213582.  
[12] F. Jiang, Y. Shan, J. Tian, L. Xu, C. Li, F. Yu, X. Cui, C. Wang, Z. Li, K. Ren, *Adv. Mater. Interfaces* **2023**, *10*, 2202474.  
[13] T. T. Le, E. J. Curry, T. Vinikoor, R. Das, Y. Liu, D. Sheets, K. T. M. Tran, C. J. Hawxhurst, J. F. Stevens, J. N. Hancock, O. R. Bilal, L. M. Shor, T. D. Nguyen, *Adv. Funct. Mater.* **2022**, *32*, 2113040.  
[14] a) M. Xu, Y. Wen, F. Niu, Q. Yang, C. Xiong, Z. Shi, *Composites, Part A* **2023**, *169*, 107518; b) H. J. Oh, D. K. Kim, Y. C. Choi, S. J. Lim, J. B. Jeong, J. H. Ko, W. G. Hahm, S. W. Kim, Y. Lee, H. Kim, B. J. Yeang, *Sci. Rep.* **2020**, *10*, 16339.  
[15] a) Z. Xiang, L. Xu, Y. Shan, X. Cui, B. Shi, Y. Xi, P. Ren, X. Zheng, C. Zhao, D. Luo, Z. Li, *Bioact Mater* **2024**, *33*, 251; b) Q. Tang, S. Sun, P. Wang, L. Sun, Y. Wang, L. Zhang, M. Xu, J. Chen, R. Wu, J. Zhang, M. Gong, Q. Chen, X. Liang, *Adv. Mater.* **2023**, *35*, 2300964.  
[16] a) Y. Zhang, S. Chen, Z. Xiao, X. Liu, C. Wu, K. Wu, A. Liu, D. Wei, J. Sun, L. Zhou, H. Fan, *Adv. Healthcare Mater.* **2021**, *10*, 2100695; b) T. Kim, H. J. Kim, W. Choi, Y. M. Lee, J. H. Pyo, J. Lee, J. Kim, J. Kim, J.-H. Kim, C. Kim, W. J. Kim, *Nat. Biomed. Eng.* **2023**, *7*, 149.  
[17] a) S. Franco-Ulloa, G. Tatulli, S. L. Bore, M. Moglianetti, P. P. Pompa, M. Cascella, M. De Vivo, *Nat. Commun.* **2020**, *11*, 5422; b) B. Y. Jiang, F. M. Feng, C. Li, M. Wang, J. Q. Xie, *Adv. Mater. Res.* **2012**, *476–478*, 1806.  
[18] X. Ma, S. Zhukov, H. von Seggern, G. M. Sessler, O. Ben Dali, M. Kupnik, Y. Dai, P. He, X. Zhang, *Adv. Electron. Mater.* **2023**, *9*, 2201070.  
[19] D. Kim, Z. Yang, J. Cho, D. Park, D. H. Kim, J. Lee, S. Ryu, S. W. Kim, M. Kim, *EcoMat* **2023**, *5*, e12384.  
[20] a) R. Hinchet, H. J. Yoon, H. Ryu, M. K. Kim, E. K. Choi, D. S. Kim, S. W. Kim, *Science* **2019**, *365*, 491; b) M. Kang, D. M. Lee, I. Hyun, N. Rubab, S. H. Kim, S. W. Kim, *Chem. Rev.* **2023**, *123*, 11559.  
[21] a) A. Sturma, L. A. Hruby, C. Prahm, J. A. Mayer, O. C. Aszmann, *Front. Neurosci.* **2018**, *12*, 906; b) N. M. Kane, A. Oware, *J. Neurol.* **2012**, *259*, 1502.